Magnon spectrum of a uniaxial antiferromagnet with a general direction of the applied field

1996 J. Phys.: Condens. Matter 8 11181

(http://iopscience.iop.org/0953-8984/8/50/040)

J. Phys.: Condens. Matter **8** (1996) 11181–11191. Printed in the UK

Magnon spectrum of a uniaxial antiferromagnet with a general direction of the applied field

Junaidah Osman†, N S Almeida‡ and D R Tilley†§

† School of Physics, Universiti Sains Malaysia, 11800 USM, Penang, Malaysia

‡ Departamento de Fisica, Universidade Federal do Rio Grande do Norte, 59072 Natal, RN, Brazil

§ Department of Physics, University of Essex, Colchester CO4 3SQ, UK

Received 24 May 1996, in final form 20 August 1996

Abstract. For a general direction of the magnetic field the sublattice moments of a uniaxial antiferromagnet deviate from antiparallel alignment along the uniaxis. The equilibrium configuration is found from the balance between exchange, anisotropy and Zeeman energies. The zero-temperature magnon spectrum for the general field direction is derived within the random-phase approximation and the results are illustrated numerically for MnF_2.

1. Introduction

The theory of a two-sublattice antiferromagnet in a zero field or with an external static field applied along the easy axis has been very extensively studied. In addition to numerous studies of the ground state, the spin-wave (magnon) spectrum and the related quantities [1] in the forms of the static and dynamic permeability tensors $\vec{\mu}(0)$ and $\vec{\alpha}(\omega)$ are well known. The expression for $\vec{\mu}(\omega)$ is used in calculations of the properties of bulk and surface retarded and magnetostatic modes [2] which are the elementary excitations for very small values of wavenumber q.

By contrast, studies of the properties when a static field is applied at a general angle θ to the easy axis are somewhat less complete. The phase diagram, and in particular the boundary between the antiferromagnetic (AF) and spin-flop (SF) phases, has been investigated by several workers; references have been given by Jones and Pankhurst [3] who reported numerical studies, based on mean-field theory, of the AF–SF boundary. In addition to uniaxial anisotropy terms $-DS_z^2$, say, giving preferred alignment along z, they included orthorhombic terms of the form $-D'S_x^2$. In a subsequent paper, Jones *et al* [4] gave an account of spin-wave theory for the antiferromagnet with uniaxial and orthorhombic anisotropy and a general direction of applied field. They used the linearized Holstein–Primakoff transformation and the Bogolubov transformation in the standard way [1] in order to find the spin-wave spectrum. Their formal results are rather general but their explicit numerical results are for the spin-wave reduction of the equilibrium value of $\langle S_z \rangle$.

As far as the permeability and related properties for general field direction are concerned, it was only in 1988 that Almeida and Mills [5] calculated $\vec{\mu}(\omega)$ for the case when the applied field is at a general angle θ to the uniaxis. They considered strictly uniaxial anisotropy, as is appropriate for the tetragonal antiferromagnets FeF_2 and MnF_2, for example, and applied random-phase-approximation (RPA) linearization to the equations of motion in order to

0953-8984/96/5011181+11$19.50

evaluate $\vec{\mu}(\omega)$. In the calculation of $\vec{\mu}(\omega)$ it is adequate to use long-wavelength ($\boldsymbol{q} = \mathbf{0}$) equations and the poles of $\vec{\mu}(\omega)$ are at the $\boldsymbol{q} = \mathbf{0}$ spin-wave energies. Almeida and Mills applied their expressions in an investigation of surface magnetostatic modes, and the extension to retarded surface modes, i.e. surface magnetic polaritons, was reported later [6]. The expressions derived in [5] have subsequently been tested experimentally in a detailed analysis of far-infrared (FIR) reflectivity spectra of FeF_2 for $\theta = 45^\circ$ [7]. More recently [8], an attenuated total reflection (ATR) stage has been added to the FIR spectrometer and used for the first observation of the surface magnetic polariton (SMP) on FeF_2 for the conventional orientation $\theta = 0^\circ$. Subsequently [9] ATR studies with a range of prism angles, still for $\theta = 0^\circ$, have been used to map out the SMP dispersion relation. These developments open the way for ATR studies for general θ and indeed the theoretical expressions needed to interpret ATR spectra are now available [6, 10, 11].

In view of this increasing activity on the $\boldsymbol{q} = \mathbf{0}$ dynamics of uniaxial antiferromagnets we return in this paper to the question of the spin-wave spectrum for general $\boldsymbol{q}$ and θ in the hope that this might stimulate further experimental work, most probably by neutron scattering. We use the simplest useful model, namely the low-temperature RPA, and we include only the exchange interaction without magnetostatic corrections. This is valid except for the region of reciprocal space very near the centre of the Brillouin zone which is inaccessible to neutron scattering. As has been stated, our formalism is a variant of that used by Jones *et al* [4] and the results that we derive are implicit within the general framework that they present. However, we use the same formalism as in our earlier work [5] so as to facilitate comparison with both theory and the FIR experimental results [7] and we present explicit formulae and numerical illustrations for the spin-wave spectrum itself. In drawing dispersion graphs we use the parameters of MnF_2 since the magnon energies for MnF_2 fall in a convenient range for neutron scattering.

The Hamiltonian and the equilibrium sublattice orientations for general θ are reviewed in section 2. In section 3 we derive the equations of motion for the spin deviations and find the magnon dispersion relation. Section 4 discusses briefly the special cases $\theta = 0^\circ$ and 90°. The results for $\theta = 0^\circ$ are well known and we simply state them for comparison; the form of the magnon spectrum for $\theta = 90^\circ$ is less well known. In section 5 we illustrate and discuss the form of the dispersion graphs, and conclusions are presented in section 6.

2. Hamiltonian and equilibrium configurations

The problem may be defined by reference to figure 1. The external field H_0 is applied at angle θ to the easy axis and we define axes z' along H_0 and z along the easy axis. Axes x and x' are as shown and the y axis is common, $y' = y$. In the presence of the field the sublattice moments are turned away from the easy axis through the angles α_1 and α_2 indicated [2]. The sign convention defined in figure 1 is the same as used previously [5], i.e. α_1 is measured clockwise from the $+z$ axis and α_2 clockwise from the $-z$ axis. In practice for MnF_2 for most values of θ and H_0 both α_1 and α_2 are negative. Since the exchange is the largest energy, for practical values of H_0 in either FeF_2 or MnF_2 the magnitudes of α_1 and α_2 are no more than a few degrees. However, $\vec{\mu}(\omega)$ is completely different from the form that it has when H_0 lies along the easy axis [2, 3] and the magnon spectrum is likewise quite different.

The Hamiltonian is

$$\mathcal{H} = \mathcal{H}_E + \mathcal{H}_A + \mathcal{H}_Z \tag{1}$$

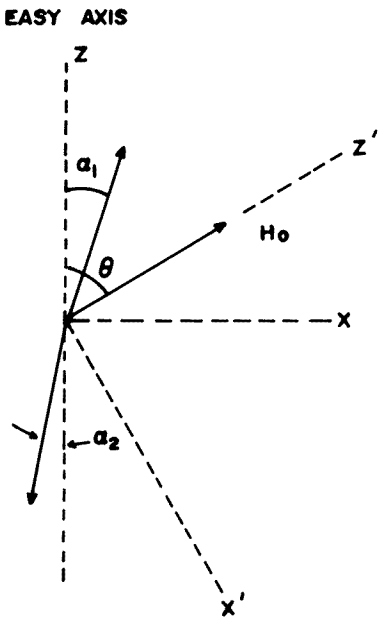

Figure 1. Geometry and axes.

where the exchange term is

$$\mathcal{H}_E = J \sum_{i,j} \boldsymbol{S}_i \cdot \boldsymbol{S}_j \tag{2}$$

with the sum over the two sublattices i and j. We assume nearest-neighbour exchange with J constant. The anisotropy and Zeeman terms are

$$\mathcal{H}_A = -D \sum_i \left(S_i^z\right)^2 - D \sum_j \left(S_j^z\right)^2 \tag{3}$$

$$\mathcal{H}_Z = -g\mu_B\mu_0 H_0 \sum_i S_i^{z'} - g\mu_B\mu_0 H_0 \sum_j S_j^{z'}. \tag{4}$$

Equations of motion are derived from (1) and it is convenient to use the primed axes of figure 1. In order to find α_1 and α_2 we use the fact that the equilibrium directions are as shown in figure 1 so that the projections along the primed axes are

$$\begin{aligned} S_i^{x'} &= -S\sin(\theta-\alpha_1) \qquad S_i^{z'} = S\cos(\theta-\alpha_1) \\ S_j^{x'} &= S\sin(\theta-\alpha_2) \qquad S_j^{z'} = -S\cos(\theta-\alpha_2). \end{aligned} \tag{5}$$

We then equate to zero the time derivatives of S_i^y and S_j^y. This gives coupled equations for α_1 and α_2, namely [5]

$$\omega_e \ \sin(\alpha_2-\alpha_1) + \omega_0 \ \sin(\theta-\alpha_1) - (\omega_a/2) \ \sin(2\alpha_1) = 0 \tag{6}$$

$$\omega_e \ \sin(\alpha_1-\alpha_2) - \omega_0 \ \sin(\theta-\alpha_2) - (\omega_a/2) \ \sin(2\alpha_2) = 0 \tag{7}$$

where

$$\omega_e = JnS \qquad \omega_a = 2DS \qquad \omega_0 = \gamma\mu_0 H_0 \tag{8}$$

n is the number of nearest neighbours and $\gamma = g\mu_B$ is 0.933 $\mathrm{cm^{-1}\ T^{-1}} = 0.1157$ meV $\mathrm{T^{-1}}$.

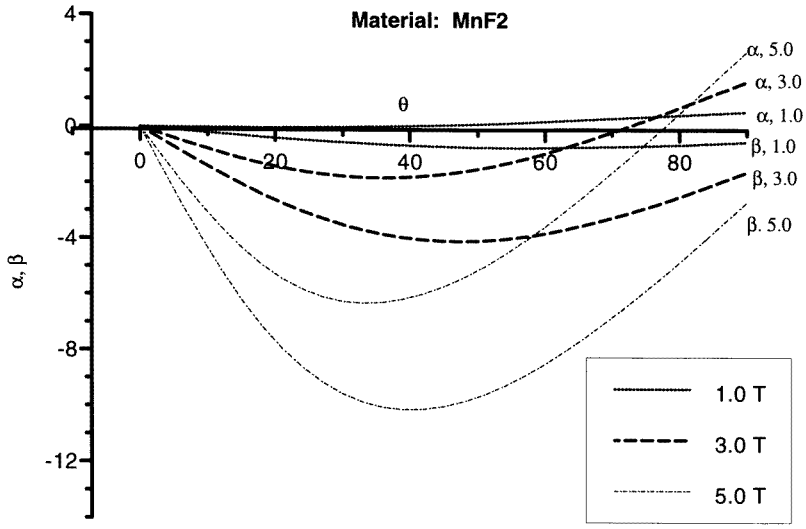

Figure 2. Solutions of (6) and (7) for the equilibrium angles α_1 and α_2 (labelled α and β respectively) in MnF_2 for applied fields of 1, 3 and 5 T.

Equations (6) and (7) apply to any equilibrium state and the solutions include an AF-like state, an SF state and a paramagnetic (P) state in which the spins are fully aligned along the direction of H_0. These different solutions may be seen in the special case $\theta = 0$ for which (6) and (7) reduce to the same known analytic form.

For general θ one may expect to find an AF-like phase, with spins near to the easy axis, for small H_0 and an SF-like phase, with spins in a distorted flop configuration, for large H_0. We consider here only the magnon spectrum in the AF phase so that we restrict attention to moderate values of H_0.

For small θ in the AF state, (6) and (7) can be linearized since α_1 and α_2 are also small. The linearization amounts only to replacing the sine functions by their arguments and the solutions of the linear equations are

$$\alpha_1/\theta = \omega_0\big(\omega_e + \omega_a + \omega_0\big)\big(\omega_a - \omega_0\big)/\big(2\omega_e\omega_a + \omega_a^2 - \omega_0^2\big) \tag{9}$$

$$\alpha_2/\theta = -\omega_0\big(\omega_e + \omega_a\big)/\big(2\omega_e\omega_a + \omega_a^2 - \omega_0^2\big). \tag{10}$$

In FeF_2 for practical values of H_0, $\omega_e > \omega_a > \omega_0$ and it follows from (9) and (10) that, for small θ, α_1 is positive and α_2 is negative [11]. In MnF_2, on the other hand, the inequalities are $\omega_e > \omega_0 > \omega_a$ so that both α_1 and α_2 are negative for small θ.

Some numerical solutions of (6) and (7) in the AF phase of MnF_2 are shown in figure 2; numerical values are [12] $\overline{h}\omega_e = 6.11$ meV and $\overline{h}\omega_a = 0.097$ meV. The linear portions near $\theta = 0$ are in agreement with (9) and (10) and the values of α_1 and α_2 for $\theta = 90^\circ$ are $\pm\alpha = \pm\sin^{-1}[\omega_0/(2\omega_e + \omega_a)]$.

3. Equations of motion and dispersion equations

In order to find the magnon spectrum we define $\sigma_i^{x'}$, etc, by

$$S_i^{x'} = Su_x + \sigma_i^{x'} \qquad S_i^{y'} = \sigma_i^{y'} \qquad S_i^{z'} = Su_z + \sigma_i^{z'} \tag{11}$$

with similar definitions on the other sublattice. Here Su_x and Su_z are the zero-order expressions defined in (5). The equations of motion are linearized in the spin deviations $\sigma_i^{x'}$, etc, and time dependence $\exp(-\mathrm{i}\omega t)$ inserted. To solve the equations we define $\beta_1^k(\boldsymbol{q})$ by

$$\sigma_i^k = N^{-1/2}\sum_{\boldsymbol{q}} \beta_1^k(\boldsymbol{q})\exp(\mathrm{i}\boldsymbol{q}\cdot\boldsymbol{r}_i) \qquad \text{for } k = x', y', z' \tag{12}$$

where N is the number of unit cells in the crystal and the sum is over values of $\boldsymbol{q}$ allowed by periodic boundary conditions. The quantity $\beta_2^k(\boldsymbol{q})$ is defined similarly in terms of a sum over the j sites. Equations for $\beta_1^k(\boldsymbol{q})$ and $\beta_2^k(\boldsymbol{q})$ are then derived in a standard way [2]. The various steps involved lead to the following: σ_i^k and σ_j^k are replaced by $\beta_1^k(\boldsymbol{q})$ and $\beta_2^k(\boldsymbol{q})$; $n^{-1}\Sigma_i\sigma_i^k$ and $n^{-1}\Sigma_j\sigma_j^k$ are replaced by $S(\boldsymbol{q})\beta_1^k(\boldsymbol{q})$ and $S(\boldsymbol{q})\beta_2^k(\boldsymbol{q})$ where $S(\boldsymbol{q}) = n^{-1}\Sigma_\delta \exp(\mathrm{i}\boldsymbol{q}\cdot\boldsymbol{\delta})$ is the usual sum over nearest-neighbour vectors δ. Thus we find that

$$\begin{aligned}-\mathrm{i}\omega\beta_1^x(\boldsymbol{q}) &= \big[\omega_0 + \omega_a\ \cos\alpha_1\ \cos\theta + \omega_e\ \cos\big(\theta-\alpha_2\big)\big]\beta_1^y(\boldsymbol{q}) \\ &\quad + \omega_e\ \cos(\theta-\alpha_1)S(\boldsymbol{q})\beta_2^y(\boldsymbol{q}) \qquad (13)\\ -\mathrm{i}\omega\beta_1^y(\boldsymbol{q}) &= -\big[\omega_0 + \omega_a\ \cos(\theta+\alpha_1) + \omega_e\ \cos\big(\theta-\alpha_2\big)\big]\beta_1^x(\boldsymbol{q}) - \big[\omega_a\ \sin\big(\theta+\alpha_1\big) \\ &\quad + \omega_e\ \sin\big(\theta-\alpha_2\big)\big]\beta_1^z(\boldsymbol{q}) - \omega_e\ \cos\big(\theta-\alpha_1\big)S(\boldsymbol{q})\beta_2^x(\boldsymbol{q}) \\ &\quad - \omega_e\ \sin\big(\theta-\alpha_1\big)S(\boldsymbol{q})\beta_2^z(\boldsymbol{q}) \qquad (14)\\ -\mathrm{i}\omega\beta_1^z(\boldsymbol{q}) &= \big[\omega_a\ \cos\alpha_1\ \sin\theta + \omega_e\ \sin\big(\theta-\alpha_2\big)\big]\beta_1^y(\boldsymbol{q}) + \omega_e\ \sin\big(\theta-\alpha_1\big)S(\boldsymbol{q})\beta_2^y(\boldsymbol{q}). \qquad (15)\end{aligned}$$

The equations for β_2^k are obtained by interchange of the subscripts 1 and 2. In addition it is necessary to change the signs of all trigonometric functions except $\cos\theta$ and $\sin\theta$. Equations (13)–(15) refer to the primed axes of figure 1 but, to simplify the notation, the primes have been dropped.

Linear spin waves are transverse in the sense that the spin-wave displacements are orthogonal to the equilibrium spin orientations. The latter are given by (5) and therefore

$$-\sin\big(\theta-\alpha_1\big)\beta_1^x(\boldsymbol{q}) + \cos\big(\theta-\alpha_1\big)\beta_1^z(\boldsymbol{q}) = 0 \tag{16}$$

and

$$\sin\big(\theta-\alpha_2\big)\beta_2^x(\boldsymbol{q}) - \cos\big(\theta-\alpha_2\big)\beta_2^z(\boldsymbol{q}) = 0 \tag{17}$$

as may be confirmed by substitution from (13) to (15) and use of (6) and (7). Because of (16) and (17) the dispersion relation is a quadratic in ω^2 as it must be for a two-sublattice antiferromagnet.

In order to derive the magnon spectrum we use (16) and (17) to eliminate $\beta_1^z(\boldsymbol{q})$ and $\beta_2^z(\boldsymbol{q})$ from the equations of motion for the x and y components. We then eliminate the y components to find the coupled linear equations

$$\omega^2\beta_1^x(\boldsymbol{q}) = P_{11}\beta_1^x(\boldsymbol{q}) + P_{12}\beta_2^x(\boldsymbol{q}) \tag{18}$$

$$\omega^2\beta_2^x(\boldsymbol{q}) = P_{21}\beta_1^x(\boldsymbol{q}) + P_{22}\beta_2^x(\boldsymbol{q}) \tag{19}$$

where

$$\begin{aligned}P_{11} &= \big[\omega_0 + \omega_a\cos\alpha_1\cos\theta + \omega_e\cos\big(\theta-\alpha_2\big)\big]\big\{\omega_0 + \omega_a\cos\big(\theta+\alpha_1\big) + \omega_e\cos\big(\theta-\alpha_2\big) \\ &\quad + \big[\omega_a\sin\big(\theta+\alpha_1\big) + \omega_e\sin\big(\theta-\alpha_2\big)\big]\tan\big(\theta-\alpha_1\big)\big\} \\ &\quad - \omega_e^2 S^2(q)\cos\big(\theta-\alpha_1\big)\big[\cos\big(\theta-\alpha_2\big) + \sin\big(\theta-\alpha_2\big)\tan\big(\theta-\alpha_1\big)\big] \qquad (20)\\ P_{12} &= S(q)\omega_e\big[\omega_0 + \omega_a\cos\alpha_1\cos\theta + \omega_e\cos\big(\theta-\alpha_2\big)\big]\big[\cos\big(\theta-\alpha_1\big) \\ &\quad + \sin\big(\theta-\alpha_1\big)\tan\big(\theta-\alpha_2\big)\big] + S(q)\omega_e\cos\big(\theta-\alpha_1\big)\big\{\omega_0 - \omega_a\cos\big(\theta+\alpha_2\big)\end{aligned}$$

$$- \omega_e \cos(\theta - \alpha_1) - \left[\omega_a \sin(\theta + \alpha_2) + \omega_e \sin(\theta - \alpha_1)\right] \tan(\theta - \alpha_2)\} \tag{21}$$

$$P_{21} = -\omega_e S(q)\left[\omega_0 - \omega_a \cos\alpha_2 \cos\theta - \omega_e \cos(\theta - \alpha_1)\right][\cos(\theta - \alpha_2) + \sin(\theta - \alpha_2)\tan(\theta - \alpha_1)\right] - S(q)\omega_e \cos(\theta - \alpha_2)\{\omega_0 + \omega_a \cos(\theta + \alpha_1) + \omega_e \cos(\theta - \alpha_2) + \left[\omega_a \sin(\theta + \alpha_1) + \omega_e \sin(\theta - \alpha_2)\right] \tan(\theta - \alpha_1)\} \tag{22}$$

$$P_{22} = \left[\omega_0 - \omega_a \cos\alpha_2 \cos\theta - \omega_e \cos(\theta - \alpha_1)\right]\{\omega_0 - \omega_a \cos(\theta + \alpha_2) - \omega_e \cos(\theta - \alpha_1) - \left[\omega_a \sin(\theta + \alpha_2) + \omega_e \sin(\theta - \alpha_1)\right] \tan(\theta - \alpha_2)\} - \omega_e^2 S^2(q) \cos(\theta - \alpha_2)\left[\cos(\theta - \alpha_1) + \sin(\theta - \alpha_1) \tan(\theta - \alpha_2)\right]. \tag{23}$$

Finally it follows from (18) and (19) that the two branches $\omega(\boldsymbol{q})$ of the magnon spectrum are the solutions of the quadratic equation

$$\omega^4 - (P_{11} + P_{22})\omega^2 + P_{11}P_{22} - P_{12}P_{21} = 0. \tag{24}$$

4. Special cases $\theta = 0^\circ$ and 90°

For $\theta = 0$ the angles α_1 and α_2 are also zero. The equations of motion (13)–(15) are readily seen to reduce to the well known form [2] and may be solved from (24) or diagonalized by use of $\beta_i^{\pm} = \beta_i^x \pm \mathrm{i}\beta_i^y$. Either way, one finds that

$$\omega = \omega_B(\boldsymbol{q}) \pm \omega_0 \tag{25}$$

where the magnon frequency in the absence of an applied field is

$$\omega_B(\boldsymbol{q}) = \left[(\omega_a + \omega_e)^2 - \omega_e^2 S^2(\boldsymbol{q})\right]^{1/2}. \tag{26}$$

The formalism also becomes easier for $\theta = 90^\circ$, i.e. H_0 transverse to the easy axis. In order to have a check on the working, we derived the results first by independent calculation and second as a special case of what we had for general θ. For $\theta = 90^\circ$ the inclinations of the sublattices are equal with α_1 and α_2 equal to $\pm\alpha$. The equations of motion separate into two sets, involving $\Sigma_{\pm}^x$, $\Sigma_{\pm}^y$ and $\Sigma_{\mp}^z$, respectively, where $\Sigma_{\pm}^k = \beta_1^k \pm \beta_2^k$. For the zone-centre modes $\boldsymbol{q} = \boldsymbol{0}$, the solvability conditions are

$$\omega^2 = \omega_r^2 \cos^2\alpha + 2\omega_e\omega_0 \sin\alpha \tag{27}$$

for the set involving Σ_+^x, etc, and

$$\omega^2 = \omega_r^2 \cos^2\alpha \tag{28}$$

for the other set. Here $\omega_r^2 = \omega_a^2 + 2\omega_a\omega_e$ defines the usual AF resonance frequency. The frequencies (27) and (28) are identical with the resonance frequencies $\Omega_\perp$ and $\Omega_\parallel$ found by Almeida and Mills [5] as the poles of $\vec{\mu}(\omega)$. It is clear from (28) that $\Omega_\parallel$ decreases as the field H_0 increases and substitution for α in (27) shows that $\Omega_\perp$ increases with increasing H_0. The existence of these two distinct resonance frequencies and their different variations with H_0 have been confirmed in FIR reflectivity experiments for $\theta = 90^\circ$ [13].

For general $\boldsymbol{q}$ we find that

$$\omega^2 = \omega_r^2 \cos^2\alpha + 2\omega_e\omega_0 \sin\alpha - \omega_e^2 D^2(\boldsymbol{q}) \cos(2\alpha) + 2\omega_e^2 D(\boldsymbol{q}) \cos^2\alpha - (2\omega_0 - \omega_a \sin\alpha)\omega_e D(\boldsymbol{q}) \sin\alpha \tag{29}$$

generalizing (27) and

$$\omega^2 = \omega_r^2 \cos^2\alpha + \omega_e^2 D(\boldsymbol{q}) \cos(2\alpha)[2 - D(\boldsymbol{q})] + \omega_e\omega_0 D(\boldsymbol{q}) \sin\alpha \tag{30}$$

generalizing (28) where $D(\boldsymbol{q}) = 1 - S(\boldsymbol{q})$. It follows that $D(\boldsymbol{q}) = 0$ at the zone centre and we show later that, for the particular case of FeF_2 or MnF_2, $D(\boldsymbol{q}) = 1$ in principal

directions at the zone edge. It is not difficult to prove that (29) and (30) give the same frequencies at the zone edge $D(\boldsymbol{q}) = 1$.

Finally we mention the $H_0 = 0$ limit of these $\theta = 90^\circ$ results. Since for $H_0 = 0$ the sublattices are aligned, $\alpha = 0$, it is evident that (27) and (28) both reduce to the AF resonance frequency ω_r. It can also be shown that both (29) and (30) reduce to $\omega^2 = [\omega_B(\boldsymbol{q})]^2$, where $\omega_B(\boldsymbol{q})$ is the zero-field magnon frequency (26).

5. Numerical illustrations

The unit cell of MnF_2 is well known [14]. The chemical cell is body-centred tetragonal but the magnetic cell is simple tetragonal with a basis comprising the oppositely directed spins at the origin and the cell centre. It is simple to evaluate $S(\boldsymbol{q})$ using for δ the eight nearest-neighbour vectors from the cell-centre spin and the result is

$$S(\boldsymbol{q}) = \tfrac{1}{4}\big[\cos\big(q_x a/2 + q_y a/2 + q_z c/2\big) + \cos\big(-q_x a/2 + q_y a/2 + q_z c/2\big) + \cos\big(q_x a/2 - q_y a/2 + q_z c/2\big) + \cos\big(q_x a/2 + q_y a/2 - q_z c/2\big)\big]. \tag{31}$$

It follows that at the Brillouin-zone edge, in the principal directions [100], [001], [110], [101] and [111], $S(\boldsymbol{q}) = 0$ while at the zone centre as usual $S(\boldsymbol{q}) = 1$. Thus the dispersion curves in all these directions can be represented as curves of ω versus $S(\boldsymbol{q})$ with the latter running from 1 to 0. For convenience we use instead $D(\boldsymbol{q})$.

Illustrative results, mapped as plots of frequency versus $D(\boldsymbol{q})$, are presented in figures 3–5. In all these figures the ordinate is $\hbar\omega$ in millielectronvolts. For $\theta = 0^\circ$ the well known result (25) is that the doubly degenerate zero-field magnon undergoes a simple Zeeman splitting that is uniform throughout the Brillouin zone. This is seen in figure 3. Figure 4 shows results for $\theta = 90^\circ$. At the zone centre $D(\boldsymbol{q}) = 0$, (27) and (28) predict a splitting of the zero-field frequency that is initially quadratic in the field strength. Numerically, it is known that for accessible fields this splitting is very small for FeF_2 [13], and figure 4 shows that despite the smaller anisotropy of MnF_2 the splitting in this case is also small. We commented earlier that at the zone edge $D(\boldsymbol{q}) = 1$, the frequencies given by (29) and (30) are the same in all fields and this is seen in figure 4.

Results for the intermediate value $\theta = 45^\circ$ are shown in figure 5. It is known [7, 11] that the zone centre frequencies show a linear Zeeman splitting that decreases as θ increases, finally vanishing at $\theta = 90^\circ$ as already seen. This decreasing Zeeman splitting is clearly seen in the comparison of figures 3 and 5 and similar curves for other intermediate values of θ. It is further seen that in the dispersion curves for 45°, like those for 0° but unlike those for 90°, the splitting continues more or less uniformly across the Brillouin zone. Our numerical results show that this holds for most intermediate values of θ except close to 90°.

6. Conclusions

Almeida and Mills [5] used the RPA to address the question of the statics and dynamics of uniaxial antiferromagnets for a general direction θ of field relative to the uniaxis and we have extended their study of the long-wavelength dynamics by finding the explicit form of the magnon dispersion throughout the Brillouin zone. Results similar to ours could have been obtained from various implicit expressions obtained by Jones *et al* [4]. The general result is given by (24) and as seen in figures 3–5 the dispersion curves for intermediate θ interpolate in a fairly regular way between the known forms for $\theta = 0^\circ$ and 90°. We have applied the RPA linearization $S_z \to \langle S_z \rangle$ and there is obviously scope for the use of more sophisticated methods.

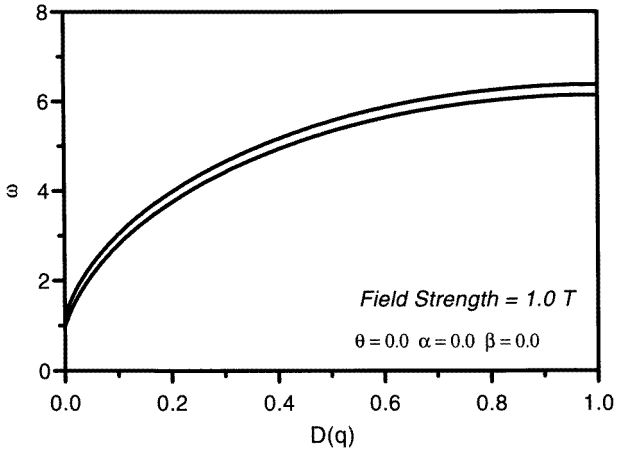

(a)

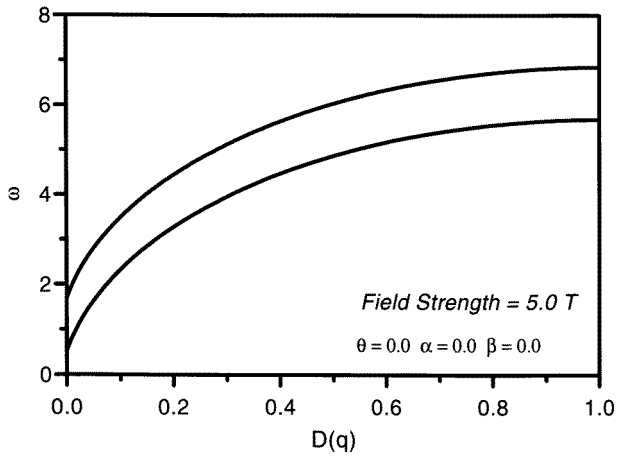

(b)

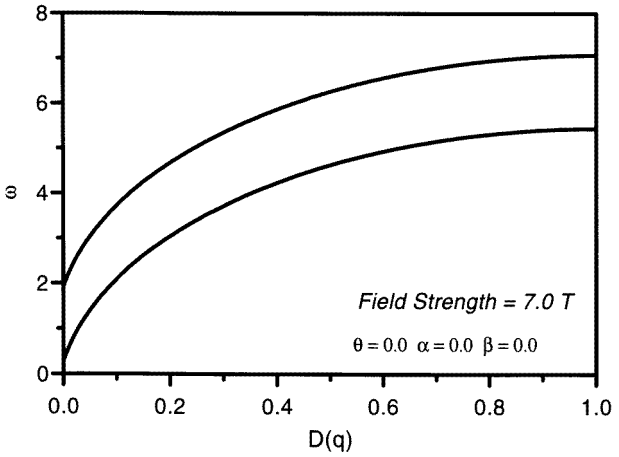

(c)

Figure 3. Magnon dispersion $\hbar\omega$ (in millielectronvolts) versus $D(\boldsymbol{q})$ for $\theta = 0^\circ$ in MnF_2. The applied fields B_0 are (a) 1 T, (b) 5 T and (c) 7 T.

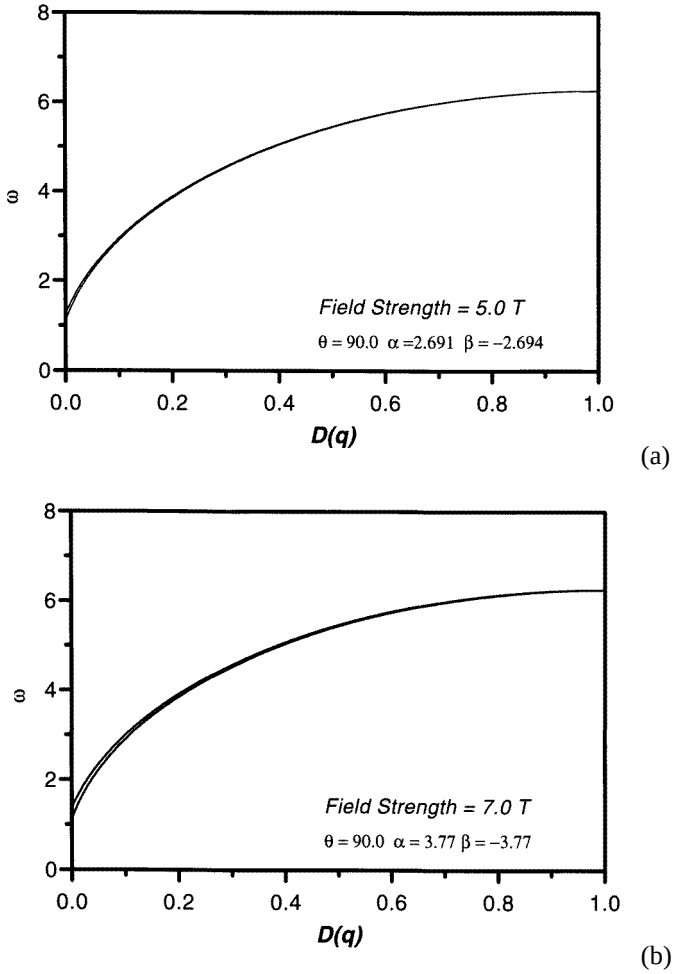

Figure 4. Magnon dispersion $\hbar\omega$ (in millielectronvolts) versus $D(\boldsymbol{q})$ for $\theta = 90^\circ$ in MnF_2. The applied fields B_0 are (a) 5 T and (b) 7 T.

We commented that the equations for the equilibrium configuration, namely equations (6) and (7), have solutions corresponding to the SF and indeed P phases as well as the AF phase that has been studied here. The equations of motion, (12)–(14), result from a linearization about equilibrium and we believe that upon substitution of the appropriate values of α_1 and α_2 they should therefore give the magnon dispersion for values of H_0 and θ for which the SF phase is stable. Thus the formalism presented here in principle enables us to study the magnon dynamics including the soft-mode behaviour across the AF–SF phase plane in H_0 and θ. Furthermore, it should be possible [15] to make use of our numerical dispersion relations to evaluate thermodynamic functions such as the Gibbs energy and specific heat in any part of the phase plane.

The present work could be used as the basis for studies of the magnon spectrum of superlattices of uniaxial antiferromagnets. Experimental studies [16, 17] of FeF_2–CoF_2 superlattices and related theoretical work [18, 19] have concentrated on equilibrium configurations. The problem of calculating an effective permeability tensor for such

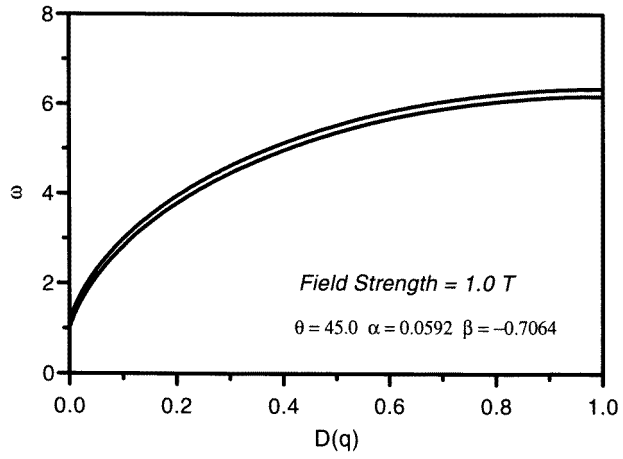

(a)

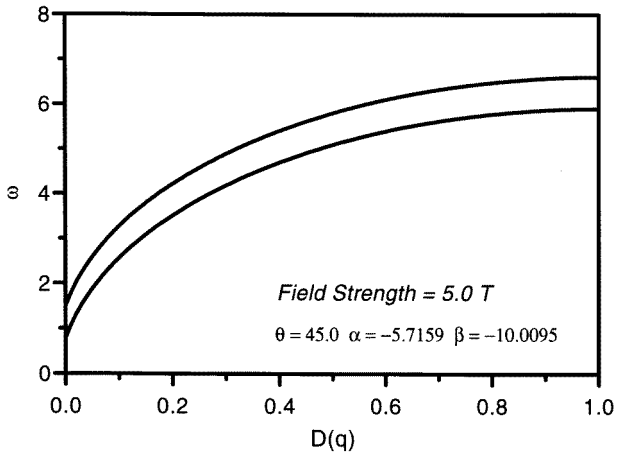

(b)

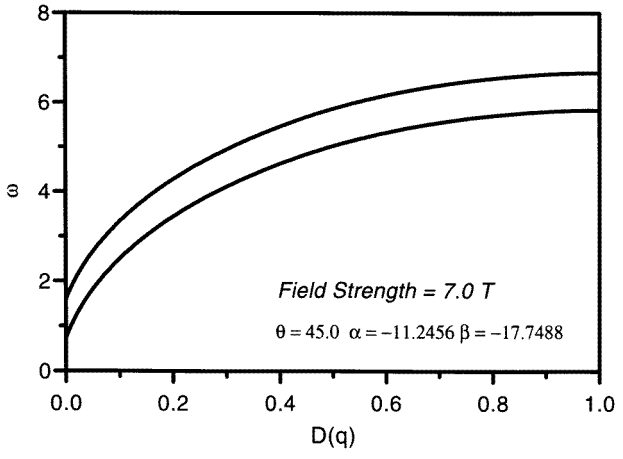

(c)

Figure 5. Magnon dispersion $\bar{h}\omega$ (in millielectronvolts) versus $D(\boldsymbol{q})$ for $\theta = 45^\circ$ in MnF_2. The applied fields B_0 are (a) 1 T, (b) 5 T and (c) 7 T.

superlattices has been addressed by Stamps and Camley [20] but as far as we know there has not yet been any study of the magnon spectrum. As is the case for ferromagnetic superlattices [21] it is necessary to understand the bulk magnon spectrum as a preliminary to deriving the superlattice spectrum.

Acknowledgments

We have benefited from useful discussions with Professor S J Joshua of the National University of Science and Technology, Bulawayo, Zimbabwe. DRT thanks the Royal Society and CNPq for a travel grant to visit Natal. The Universiti Sains Malaysia part of this work was supported by university research grants to JO and DRT.

References

[1] Mattis D C 1981 *The Theory of Magnetism I: Statics and Dynamics* (Berlin: Springer)
[2] Cottam M G and Tilley D R 1989 *Introduction to Surface and Superlattice Excitations* (Cambridge: Cambridge University Press)
[3] Jones D H and Pankhurst Q A 1987 *J. Phys. C: Solid State Phys.* **20** 2453
[4] Jones D H, Pankhurst Q A and Johnson C E 1987 *J. Phys. C: Solid State Phys.* **20** 5149
[5] Almeida N S and Mills D L 1988 *Phys. Rev.* B **37** 3400
[6] Fonseca T L, Carriço A S and Almeida N S 1992 *Phys. Rev.* B **46** 11 626
[7] Kamsul Abraha, Brown D E, Dumelow T, Parker T J and Tilley D R 1994 *Phys. Rev.* B **50** 6808
[8] Jensen M R F, Parker T J, Kamsul Abraha and Tilley D R 1995 *Phys. Rev. Lett.* **75** 3756
[9] Jensen M R F, Feiven S A, Parker T J and Camley R E 1996 *Phys. Rev. Lett.* submitted
[10] Kamsul Abraha 1995 *PhD Thesis* University of Essex
[11] Kamsul Abraha and Tilley D R 1996 *Surf. Sci. Rep.* **219** 1
[12] Sanders R W, Belanger R M, Motokawa M, Jaccarino V and Rezende S M 1981 *Phys. Rev.* B **23** 1190
[13] Brown D E, Dumelow T, Parker T J, Kamsul Abraha and Tilley D R 1994 *Phys. Rev.* B **49** 12 266
[14] Cottam M G and Lockwood D J 1986 *Light Scattering in Magnetic Solids* (New York: Wiley)
[15] Joshua S J 1996 private communication
[16] Ramos C A, Lederman D, King A R and Jaccarino V 1990 *Phys. Rev. Lett.* **65** 2913
[17] Lederman D, Belanger D P, Wang J, Han S-J, Paduani C, Ramos C A and Nicklow R M 1993 *Mater. Res. Soc. Symp. Proc.* **313** 333
[18] Carriço A S and Camley R E 1992 *Phys. Rev.* B **45** 13 117
[19] Wang R W and Mills D L 1992 *Phys. Rev.* B **46** 11 681
[20] Stamps R L and Camley R E *Phys. Rev.* B at press
[21] Albuquerque E L, Fulco P, Sarmento E F and Tilley D R 1986 *Solid State Commun.* **58** 41